Sodium diffusion in alkali feldspars: Towards the impact of Al/Si ordering

Olga Kulitckaya,[1] Alexander Gorfer,[2] Elena Petrishcheva,[2] Bengü Tas,[1]
Vladislav Kulitckii,[1] Gerhard Wilde,[1] Rainer Abart,[2] and Sergiy V. Divinski[1]

[1] *Institute of Materials Physics, University of Münster, 48149 Münster, Germany*
[2] *Department für Lithosphärenforschung, University of Vienna, 1090 Wien, Austria*

(Dated: December 17, 2024)

Tracer diffusion of Na in natural alkali feldspars including sanidine, adularia and orthoclase with different Na:K ratios is measured using the radiotracer technique and applying the ^{22}Na radioisotope. The tracer diffusion measurements along the crystallographic directions $\perp(001)$ and $\perp(010)$ in alularia feldspar reveled a slight (within a factor of two to three) anisotropy of Na diffusion with the faster diffusion rates along the $\perp(001)$ directions, while this difference was less prominent in orthoclase. The anisotropy of Na diffusion is specifically addressed for orthoclase and the full diffusion tensor is determined. The impact of temperature and composition on diffusion in natural alkali feldspars is discussed with respect to impurities and intrinsic defects. The state of Al/Si ordering is proposed to have a significant influence on the Na diffusion rates in alkali feldspars.

Keywords: Tracer diffusion; alkali feldspar; potassium feldspar; sanidite; adularia; orthoclase

I. INTRODUCTION

Alkali feldspar is one of the most common minerals in the Earth's crust occurring in magmatic, metamorphic, and sedimentary rocks, and its properties are of high interest in Earth science [1, 2]. For example, the coarsening of exsolution lamellae in alkali feldspar, which is controlled by alkali diffusion, is used for reconstructing the thermal history of the feldspars and their host rocks [3–7]. Reliable and extended data on alkali cation diffusion in the alkali feldspars are thus of considerable interest [8].

The alkali feldspars form a solid solution between the Na end-member albite ("Ab" = $NaAlSi_3O_8$) and the K end-member K-feldspar ("Ksp" = $KAlSi_3O_8$). The composition of an alkali feldspar solid solution along the binary join between these two end-members is expressed as $X_K = z_K/(z_K + z_{Na})$, where z_K and z_{Na} are the site fractions of K and Na on the alkali sites in molar units. The crystal structure of alkali feldspar is comprised of a three dimensional framework of corner-sharing SiO_4 and AlO_4 tetrahedra, and the alkali cations occupy large cavities within the tetrahedral framework. Four different tetrahedral positions can be discerned: T_1m, T_1o, T_2m, T_2o, see Fig. 1. In disordered alkali feldspar, Al and Si are randomly distributed over all four tetrahedral sites. In alkali feldspar with intermediate ordering, Al is preferentially partitioned into the T_1 sites, where $T_1 = T_1m + T_1o$. In fully ordered alkali feldspar, Al is preferentially partitioned into the T_1o sites, as sketched in Fig. 1. In this case, AlO_4 and SiO_4 tetrahedra alternate along the [110] crystallographic direction, whereas chains of SiO_4 tetrahedra appear along the $1\bar{1}0$ direction.

Based on the degree of Al/Si ordering, the Na end-member may be classified as high albite (fully disordered), intermediate albite (intermediate ordering state), and low albite (fully ordered). Similarly, the K end-member may be classified as sanidine (fully disordered), orthoclase (intermediate ordering state) or microcline (fully ordered) [10]. At high temperatures, the alkali feldspars show complete miscibility. Below about 600°C, depending on the state of Al/Si ordering and on minor element contents, a miscibility gap opens, and when alkali feldspar of intermediate composition enters the two-phase region of the phase diagram due to cooling, it tends to exsolve, typically forming a lamellar intergrowth of more Na-rich and more K-rich alkali feldspar, a microstructure referred to as perthite [2]. After their initial formation, the lamellae undergo coarsening, and calibration of the respective coarsening kinetics is crucial for the determination of geological cooling rates [11]. So far, the accuracy of reconstructions of the thermal history from perthites has been limited [11], especially because calibration of the relevant kinetic processes was mainly based on segregation experiments, which integrate all underlying processes, including diffusion of alkali cations, formation of new phase boundaries, and thermodynamic driving forces, including their modification due to elas-

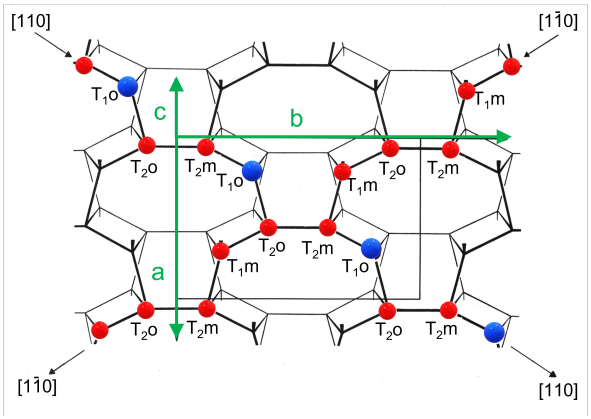

FIG. 1. Projection of the idealized feldspar structure on the (001) crystallographic plane (modified after Laves [9]). The T-sites are the centers of the Si–O (red spheres) or Al–O (blue spheres) tetrahedra. A fully ordered Al/Si state is sketched. The principle crystallographic directions are shown.

tic energy arising from coherent lamellar intergrowth. In order to better understand diffusive phase transformations in alkali feldspar, the underlying kinetic processes, in particular diffusion of the alkali cations, need to be calibrated independently.

Diffusion of alkali cations in alkali feldspars has been investigated over several decades [1, 12], but still bears a number of unresolved problems. Fundamental questions have arisen with work on Na–K interdiffusion, which reveals systematic differences between the experimentally determined Na–K interdiffusion coefficients and those calculated from combining the experimentally determined Na and K self(tracer)-diffusion coefficients from the literature with a thermodynamic assessment within the framework of the available interdiffusion models [2, 13]. The tracer diffusion coefficients of Na and K in alkali feldspars were measured for a few selected specimens [14–17]. Experiments on Na diffusion revealed an anisotropy of Na self (tracer) diffusion, though relatively small, within a factor of 3 [18]. Moreover, as a general trend, an enhancement of Na diffusion with increasing K content was elucidated and explained in terms of vacancy-mediated jumps of alkali atoms as the main diffusion mechanism [14, 18]. Frenkel pairs were proposed to be the major point defects in alkali feldspar, because the high Si–O bonding energies make the formation of Schottky defects extremely unfavourable [17]. In general, the vacancy mechanism and the interstitialcy mechanism should therefore be considered as dominant in alkali diffusion processes.

Alongside with the chemical composition, X_{K}, and the minor element concentrations such as Ba and Ca on the alkali sites, the degree of Al/Si ordering may influence the physical properties of alkali feldspar in thermodynamic equilibrium and its kinetic behavior [19]. For example, the critical temperature of the solvus curve is considerably higher for alkali feldspar with a high degree of Si/Al ordering than for disordered ones [20]. Moreover, substitutional Al/Si ordering was found to influence strongly the dissolution stoichiometry [21], although Liu and Zhai [22] concluded that the degree of Al/Si ordering does not impose any measurable effect on the dissolution of K-feldspars. Generally, the degree of Al/Si ordering depends on temperature and composition [19] and the influence of the Al/Si ordering on the diffusion of alkali cations is not well understood.

The present paper extends the previously reported Na tracer diffusion measurements towards a broader series of alkali feldspars including orthoclase ($Or_{95}Ab_5$), adularia ($Or_{85}Ab_{15}$) and two types of sanidine with ($Or_{83}Ab_{15}Cs_1$ and $Or_{71}Ab_{26}Cs_2$), where Cs indicates Celsian ($BaAl_2Si_2O_4$) component. Despite of having relatively similar chemical compositions, the investigated adularia and sanidine show significantly different Na diffusion rates. Moreover, with respect to the Na diffusion rates, the feldspars are shown to form two distinct branches indicating a potential impact of Al/Si ordering on alkali cation diffusion. Finally, the anisotropy of Na diffusion in Madagascar orthoclase is carefully measured and the full diffusion tensor is extracted.

II. EXPERIMENTAL PROCEDURE

A. Materials

Four natural alkali feldspars with different compositions and different Al/Si ordering states were used for radiotracer diffusion experiments. All feldspars are monoclinic with space group C2/m. For monoclinic alkali feldspar, the degree of Al/Si ordering may be expressed as $2t_1$, where t_1 indicates the proportion of Al-ions on each of the T1 sites. For fully disordered alkali feldspar t_1=0.25 and for intermediate ordering state t_1=0.5. Listed according to the increasing K concentration and with the $2t_1$ values taken from [20], the alkali feldspars used in this study are:

(i) Sanidine from the Eifel region Rockeskyll, Germany (RK) with end-member mole fractions of $Or_{71}Ab_{26}Cs_2$ and with a minor FeO concentration of about 0.1 to 0.2 wt.%

(ii) Sanidine from the Eifel region Volkesfeld (VF) with end-member mole fractions of $Or_{83}Ab_{15}Cs_1$, with $2t_1$=0.611, and with a similar FeO concentration as the RK sanidine

(iii) Adularia from Zillertal (AZ) with end-member mole fractions of $Or_{85}Ab_{15}$ and with $2t_1$=0.838

(iv) Orthoclase from Madagascar (MO) with end-member mole fractions of $Or_{95}Ab_5$, with $2t_1$=0.689, and with low Ba concentration and about 1 wt.% of FeO

The chemical compositions of the studied feldspars expressed in terms of atoms per formula unit corresponding to the formula (Na,K)$AlSi_3O_8$) are given in Table I.

TABLE I. Chemical compositions of the studied alkali feldspars in atoms per formula unit (Na,K)$AlSi_3O_8$.

Element	MO	AZ	VF	RK
Si	3.02	2.971	2.98	2.97
Al	0.93	1.030	1.02	1.02
Ti	0.00	–	0.00	0.00
Fe	0.04	–	0.01	0.01
Mg	0.00	–	0.00	0.00
Ca	0.00	0.001	0.00	0.00
Na	0.05	0.146	0.15	0.26
K	0.95	0.837	0.83	0.71
Rb	–	–	0.00	–
Ba	0.00	0.015	0.01	0.02
Sr	–	–	0.00	0.01
O	8.00	8.00	8.00	8.00

B. Sample preparation

Centimetre-sized pieces of large single crystals were cleaved along the (001) and (010) cleavage planes. The crystallographic orientations of the cleaved pieces were determined on a four circle single crystal X-ray goniometer and machined to 1.5 to 2.0 mm thick plates featuring an octagonal base plane with a diameter of $\geq$ 5 mm, which was oriented parallel to either the (001) or (010) plane. In the case of Madagascar orthoclase, single crystal plates with their basal plane parallel to the (110), $(\bar{1}01)$, and $(01\bar{1})$ planes as well as perpendicular to the [101] direction were prepared in addition.

The surface plane was polished with diamond paste down to 0.25 µm using a standard polishing procedure. Afterwards, the samples were annealed in a purified Ar atmosphere at 1373 K for 24 h for stress relaxation.

C. Radiotracer method

A standard radiotracer technique was used to determine the sodium self-diffusion coefficients [23]. A few microliters of a highly diluted solution of the radioisotope ^{22}Na (half-time of 950 days) were applied on the polished sample surface and dried under an infrared lamp. The samples were packed in a tantalum foil, sealed into silica glass tubes under a purified Ar atmosphere and diffusion annealed. Annealing measurements were performed in the temperature range from 603 K to 1173 K.

The penetration profiles were determined by two different sectioning methods, namely by parallel mechanical sectioning using a precision grinding device or by ion-beam sputtering. With mechanical grinding, penetration profiles longer than about 10 µm were determined, and with ion-beam sputtering, penetration depths shorter than about 1 to 4 µm were reliably resolved. For analysing penetration profiles from annealing experiments done at temperatures below 900 K, the ion-beam sputtering (IBS) technique was used. This combination of sectioning methods allowed experiments from a broad temperature range to be reliably analyzed and, through this, to improve the accuracy of the inferred Arrhenius parameters.

The mechanical sectioning via grinding was done using a Mylar foil with 30 µm sized SiC particles. For each section the mass of the abraded material was determined by weighing the sample to an accuracy of ±0.1 µg on a microbalance before and after the sectioning step.

In the case of ion-beam sputtering, the total removed depth was determined by weighing the samples before and after sputtering on the same microbalance. The section thicknesses were estimated assuming a constant sputtering rate, the stability of which was controlled by recording the sputtering current. Further details on the ion-beam sputtering procedure can be found in Ref. [23].

A well-type NaI-detector was used for the measurement of the radioactivity of the individual sections following the intensity of the 512 keV line. The penetration profiles correspond to the plots of the specific radioactivity of the successive sections, i.e. the background-subtracted radioactivity divided by the section mass, vs. the penetration depth.

III. RESULTS AND DISCUSSION

A. Na diffusion in MO and AZ feldspars

The penetration profiles measured for ^{22}Na diffusion perpendicular to the (001) and (010) crystallographic planes in Madagaskar orthoklase (MO) and Zillertal Adularia (AZ) are shown in Fig. 2, where the relative specific activity, which is proportional to the tracer concentration, is plotted versus penetration depth squared, x^2.

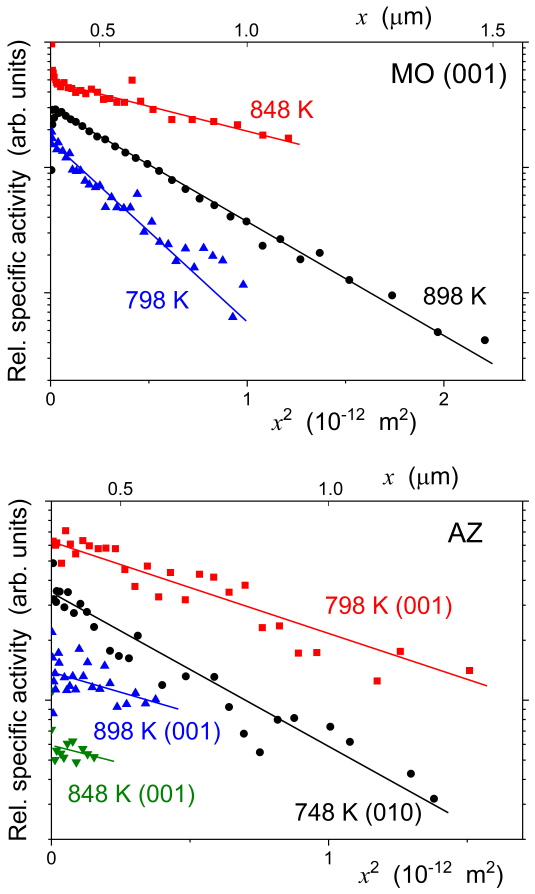

FIG. 2. Examplary penetration profiles from ^{22}Na diffusion in (a) Madagaskar orthoklase and (b) Zillertal adularia measured using the IBS method

The measured tracer distributions are well approximated using the Gaussian solution of the diffusion problem, see the solid lines in Fig. 2. In such case, the logarithm of the tracer concentration decays linearly with penetration depth squared, x^2. The determined tracer

diffusion coefficients, D^*,

$$D^* = \frac{1}{4t}\left(-\frac{\partial \bar{C}(x)}{\partial x^2}\right)^{-1}, \qquad (1)$$

are listed in Table II. Here $\bar{C}(x)$ is the tracer concentration at depth x.

At temperatures above 900 K, the mechanical sectioning technique was used to determine the ^{22}Na penetration profiles. Examples of the measured profiles at $T = 1098$ K are shown in Fig. 3. The penetration profiles were approximated by the Gaussian solution of the diffusion problem and the determined tracer diffusion coefficients are given in Table II.

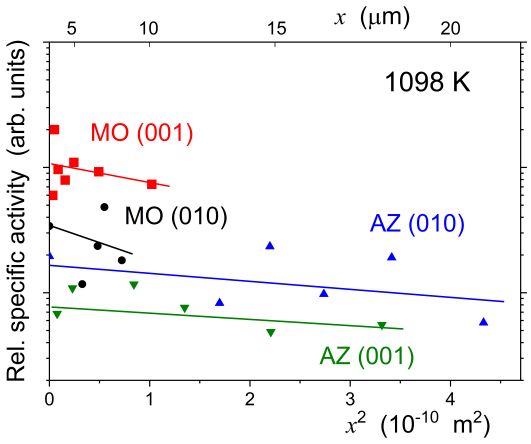

FIG. 3. Penetration profiles of ^{22}Na from diffusion in Madagaskar orthoklase and Zillertal adularia measured by the mechanical sectioning method.

In Fig. 4, the tracer diffusion coefficients, D^*, measured for the MO and AZ feldspars are plotted versus the inverse absolute temperature T. Figure 4 suggests that the diffusion anisotropy of Na diffusion in adularia is measurable, with the Na diffusion rates along the $\perp(001)$ crystallographic direction being higher than those along the $\perp(010)$ direction by a factor of two to three, while the Na diffusion rates along these directions in the Madagascar orthoclase (MO) are almost similar.

B. Diffusion anisotropy in Madagascar orthoclase

The anisotropy of Na diffusion in Madagascar orthoclase was assessed in more detail combining the measurements along six different crystallographic directions, $\perp(001)$, $\perp(010)$, $\perp(110)$, $\perp(\bar{1}01)$, $\perp(01\bar{1})$, $\|[101]$. The main crystallographic directions of a feldspar are schematically shown in Fig. 5.

The experimental results for Na diffusion in the Madagascar orthoclase are summarized in Table II. The tracer diffusion coefficients obtained from these data are plotted in Fig. 6 in the Arrhenius coordinates. The corresponding Arrhenius parameters are given in Table III.

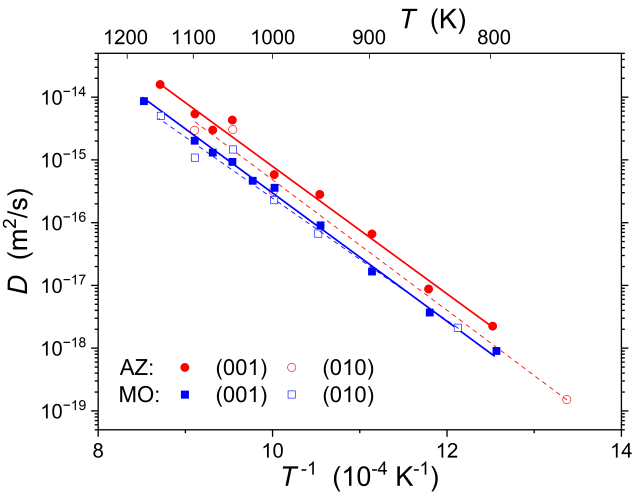

FIG. 4. Arrhenius plots for Na diffusion in MO (red symbols) and AZ (blue symbols) feldspars along the normal directions to the (001) (filled symbols and solid lines) and (010) (open symbols and dashed lines) lattice planes. The lines represent the corresponding Arrhenius fits.

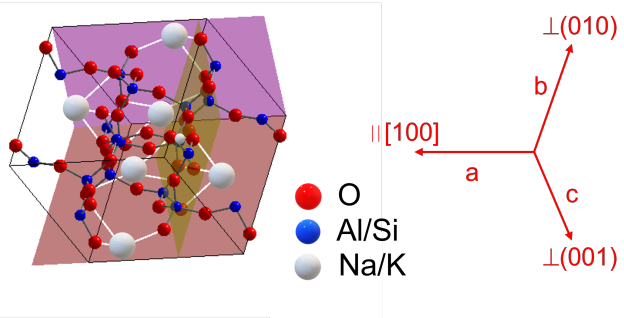

FIG. 5. Main crystallographic planes and site occupation in a Na/K feldspar. The (010), (001) and $(19, 0, \bar{7})$ planes are indicated in violet, red and yellow, respectively. The $(19, 0, \bar{7})$ plane is perpendicular to the [100] direction.

From these data, the diffusion tensor corresponding to Na tracer diffusion in MO can be extracted. We follow the procedure described by Petrishcheva et al. [24]. The effective diffusivity along an arbitrary direction $\mathbf{n}$, which is specified by its directional cosines $\mathbf{n} = (n_1, n_2, n_3)$, is given by

$$D_n = \sum_{i,j} D_{ij} n_i n_j, \qquad i, j = 1, 2, 3, \qquad (2)$$

where D_{ij} are the components of the diffusivity tensor. The diffusivity tensor refers to the coordinate system generated by ($\boldsymbol{a}$, $\boldsymbol{b}$, $\boldsymbol{c}^*$), where $\boldsymbol{b}$ is set parallel to the crystallographic dyad axis and $\boldsymbol{c}^* = \boldsymbol{a} \times \boldsymbol{b}$. For the monoclinic symmetry at hand, the tensor takes the form

$$D_{ij} = \begin{pmatrix} D_{11} & 0 & D_{13} \\ 0 & D_{22} & 0 \\ D_{13} & 0 & D_{33} \end{pmatrix}.$$

TABLE II. Measured diffusion coefficients (in m^2/s) of ^{22}Na diffusion in the studied alkali feldspars for the given crystallographic directions. At some temperatures, the measurements were performed several times to check the reliability of the data. The uncertainties of the determined tracer diffusion coefficients are typically less than 15%.

T (K)	Material							
	MO						AZ	
	$\perp$ (001)	$\perp$ (010)	$\perp$ (110)	$\perp$ ($\bar{1}$01)	$\perp$ (01$\bar{1}$)	$\parallel$ [101]	$\perp$ (001)	$\perp$ (010)
1173	1.09×10^{-15}	8.83×10^{-15}	2.90×10^{-15}	3.68×10^{-15}		9.28×10^{-15}		
	8.6×10^{-15}							
1150		5.0×10^{-15}					1.6×10^{-14}	
1123	5.34×10^{-15}	4.87×10^{-15}	1.77×10^{-15}*	1.49×10^{-15}		3.81×10^{-15}	5.4×10^{-15}	3.0×10^{-15}
1100	2.0×10^{-15}	1.1×10^{-15}					5.4×10^{-15}	3.0×10^{-15}
1073	1.3×10^{-15}						3.0×10^{-15}	
	2.68×10^{-15}	1.85×10^{-15}	5.03×10^{-16}	6.70×10^{-16}	1.28×10^{-15}	1.60×10^{-15}	3.0×10^{-15}	
1050	9.3×10^{-16}	1.5×10^{-15}					4.3×10^{-15}	3.0×10^{-15}
1023	4.77×10^{-16}	5.69×10^{-16}	1.73×10^{-16}	3.56×10^{-16}	3.75×10^{-16}	3.88×10^{-16}		
	4.6×10^{-16}							
1000	3.6×10^{-16}	2.3×10^{-16}					5.8×10^{-16}	3.2×10^{-16}
973	1.94×10^{-16}	9.08×10^{-17}	4.97×10^{-17}	1.47×10^{-16}	9.83×10^{-17}	1.57×10^{-16}		
950	9.1×10^{-17}	6.7×10^{-17}					2.8×10^{-16}	
923	4.93×10^{-17}	2.13×10^{-17}	5.46×10^{-17}	4.65×10^{-17}	2.46×10^{-17}	6.63×10^{-17}		
900	1.7×10^{-17}	1.88×10^{-17}	2.17×10^{-17}	2.28×10^{-17}	1.93×10^{-17}	2.28×10^{-17}		
873	1.44×10^{-17}							
850	3.7×10^{-18}						8.7×10^{-18}	
823	2.23×10^{-18}	2.95×10^{-18}	2.51×10^{-18}	3.28×10^{-18}	3.18×10^{-18}	1.90×10^{-18}		
		2.1×10^{-18}						
800	9.0×10^{-19}						2.2×10^{-18}	
773	4.60×10^{-19}	5.03×10^{-19}	5.54×10^{-19}	1.00×10^{-18}	2.43×10^{-19}	8.57×10^{-19}		
750								1.5×10^{-19}

* the exact temperature was 1125 K

The values of D_n were measured along the specified directions over a range of temperatures and then approximated for the two temperatures, 773 K and 1173 K, using the corresponding Arrhenius equations,

$$D_n = D_0^{(n)} \exp(-Q_n/RT), \tag{3}$$

where the pre-factors, $D_0^{(n)}$, and the activation enthalpies, Q_n, for Na diffusion in the MO feldspar along the six directions

$$\perp(001), \quad \perp(010), \quad \perp(110), \quad \perp(\bar{1}01), \quad \perp(01\bar{1}), \quad \parallel[101]$$

were taken from Table III.

The directional cosines are calculated using the unit cell parameters from [25] for the MO feldspar mole fraction, $X_K = 0.95$. The data on D_n from Table III and Eq. (2) were used to assess the unknown components of the diffusivity tensor D_{ij}. Our results for the components of the diffusivity tensor at 773 K and 1173 K are shown in Table IV, and the corresponding characteristic ellipsoids

$$D_{11}X^2 + D_{22}Y^2 + D_{33}Z^2 + 2D_{13}XZ = \text{const}$$

are plotted in the abstract (X, Y, Z) space in Fig. 7a,b. The constant has been chosen so that the characteristic ellipsoid is inscribed in a unit sphere.

From the eigenvalues of D_{ij}, the maximum anisotropy, i.e., the ratio of the diffusion coefficients for the fastest and slowest diffusion directions, is close to 3 at $T = 773$ K and it reaches about 30 at $T = 1173$ K. The change in the shape of the characteristic ellipsoid from an oblate one at $T = 773$ K to a prolate one at $T = 1173$ K reflects the different activation energies for Na tracer diffusion in different directions (see Fig. 6, Table III). It is interesting to note that the activation energies for directions within the (100) plane, i.e., $\perp(001), \perp(010), \perp(01\bar{1})$, are systematically higher than the activation energies

TABLE III. Pre-factor, D_0, and activation enthalpy, Q, of ^{22}Na diffusion in alkali feldspars along the selected crystallographic directions.

Material	Direction	D_0	Q	Ref.
		10^{-8} m^2/s	kJ/mol	
AZ	$\perp$ (001)	1230^{+1890}_{-739}	195 ± 8	
AZ	$\perp$ (010)	1370^{+9170}_{-119}	199 ± 16	
MO	$\perp$ (001)	368^{+188}_{-125}	192 ± 4	present work
MO	$\perp$ (010)	145^{+209}_{-86}	186 ± 8	
MO	$\perp$ (110)	$2.23^{+4.7}_{-1.5}$	156 ± 10	
MO	$\perp$ ($\bar{1}$01)	$2.13^{+1.38}_{-0.84}$	153 ± 4	
MO	$\perp$ (01$\bar{1}$)	89.2^{+372}_{-72}	183 ± 12	
MO	$\parallel$ [101]	68.1^{+91}_{-39}	178 ± 7	
VF	$\perp$ (001)	$8.0^{+2.4}_{-1.9}$	123 ± 3	[14]
VF	$\perp$ (010)	$5.8^{+4.4}_{-2.5}$	122 ± 4	[14]
RK	$\perp$ (001)	$2.55^{+1.45}_{-0.92}$	117 ± 4	[16]
RK	$\perp$ (010)	$1.71^{+0.68}_{-0.49}$	115 ± 3	[16]
MO	$\parallel$ [010]	210^{+260}_{-120}	198 ± 7	[16]

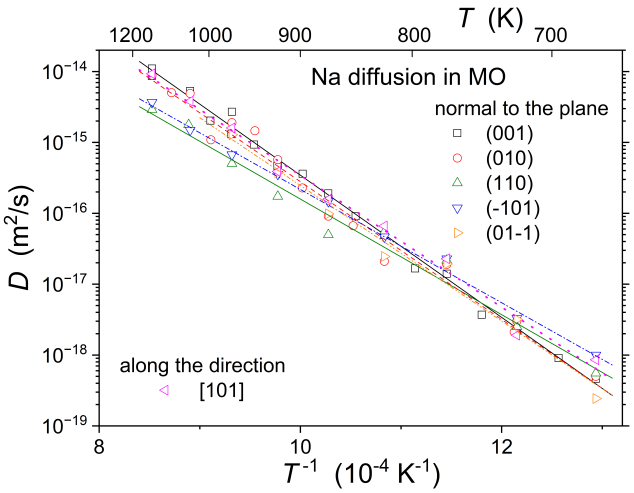

FIG. 6. Anisotropy of Na diffusion in Madagaskar orthoklase [15] as measured perpendicular to the five specified crystallographic planes and along the [101] crystallographic direction.

for directions pointing out of the (100) plane, i.e., $\perp(110), \perp(\bar{1}01), \parallel[101]$, indicating probably contributions of several concurrent microscopic mechanisms governing Na diffusion.

TABLE IV. Components of the diffusivity tensor D_{ij} in 10^{-17}m^2/s units.

	773 K	1173 K
D_{11}	0.108	48
D_{22}	0.036	708
D_{33}	0.041	871
D_{13}	-0.013	123

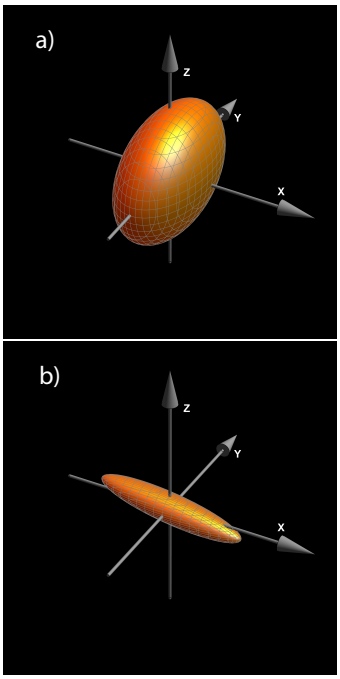

FIG. 7. Characteristic surfaces for two diffusivity tensors: a) $T = 773$ K and b) $T = 1173$ K.

C. Temperature dependence of Na diffusion in alkali feldspar

In Fig. 8, the Na tracer diffusion coefficients for MO and AZ from this study are compared with the literature data on Na diffusion in various alkali feldspars. The reported Arrhenius parameters are listed in Table III.

Over the investigated temperature range, the measured tracer diffusion coefficients follow generally Arrhenius-type temperature dependencies. It is evident that the activation energies of Na diffusion are about (190±10) kJ/mol for MO and AZ feldspars, whereas they are about (120 ± 5) kJ/mol for the RK and VF feldspars. Noting that MO ($X_K = 0.93$) is more K rich than VF ($X_K = 0.83$), the comparatively high activation energy for Na diffusion in MO as compared to the activation energy for Na diffusion in VF was ascribed to the increasing necessity of K jumps to allow for Na diffusion with

increasing X_K [14, 18]. This reasoning does, however, not hold for the comparison of the activation energies between VF and AZ, as these feldspars have nearly the same major element composition, (VF: $X_K = 0.83$, AZ: $X_K = 0.85$). A different mechanism might be responsible for explaining the difference in activation energies between these two feldspars.

In order to test the reproducibility of the present results for the MO and AZ feldspars, we performed exemplary measurements of Na diffusion in VF and RK minerals at 700 K. The determined tracer diffusion coefficients are 9.9×10^{-17} m^2/s and 3.0×10^{-17} m^2/s, respectively, and these results are shown in Fig. 8, black and green stars. A perfect agreement with the literature data, Refs. [14, 16], is seen indicating a very good reliability of all datasets.

D. Controls on Na diffusion in alkali feldspar

Based on the measured Na diffusivities, the studied alkali feldspars can be divided into two groups, with VF and RK belonging to one group and MO and AZ constituting another group. This fact is exciting, because these feldspars cover the compositional range $0.71 \leq X_K \leq 0.94$. Moreover, the major element compositions of the VF ($X_K = 0.83$) and the AZ ($X_K = 0.85$) feldspars are very similar (Table I), but the Na diffusivities differ by orders of magnitude between VF and AZ, especially at low temperatures, Fig. 8.

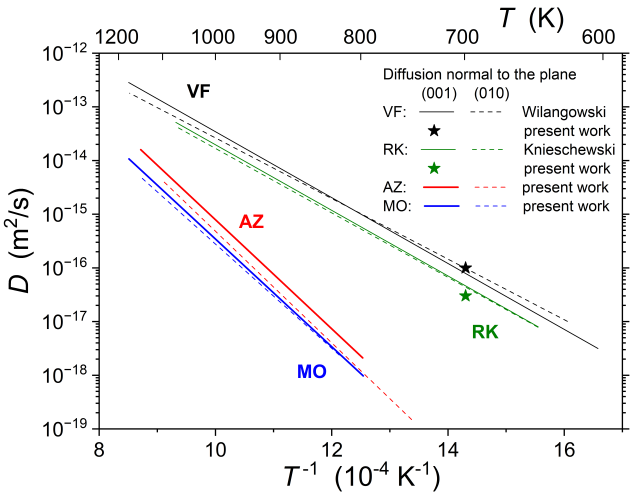

FIG. 8. Na diffusion in alkali feldspars along the directions normal to the (001) (solid lines) and normal to (010) (dashed lines) crystallographic planes. The present data on MO (blue) and AZ (red) minerals are compared with the data reported on VF by Wilangowski [14] (blue) and on RK by Knieschwski [16] (green). The present results of single measurements of Na diffusion in VF (black) and RK (green) are shown by stars.

Three main factors need to be scrutinized in order to improve our understanding of the differences in Na diffusivities between these feldspars:

(i) The major element composition as expressed by X_K;

(ii) The contents of minor and trace element such as Rb, Ca, Ba or Sr, which may be involved in homovalent and heterovalent substitutions on the alkali sites;

(iii) The degree of Al/Si ordering in the tetrahedral framework.

Due to the high binding energy of the Si–O bonds, Shottky defects are very unlikely in alkali feldspar, and Frenkel pairs, comprised of a vacancy on the alkali site and an alkali cation on an interstitial site, are considered as the most important type of point defect in alkali feldspar [26]. Thus, the vacancy mechanism and diffusion via interstitial positions should be considered.

Feldspar composition, X_K. It was shown by means of Monte Carlo simulations [18] that in K-rich alkali feldspars the self-diffusion coefficients of Na and K cannot differ by more than a factor of about 3, if alkali diffusion occurs by the vacancy mechanism. In K-rich alkali feldspar, experimentally determined Na and K self diffusion coefficients differ by three orders of magnitude at 900°C, indicating that interstitials are the most important vehicles for alkali diffusion in alkali feldspar rather than the vacancies [17].

Based on the notion that the larger K ion is less mobile than the comparatively small Na ion, it was inferred by Wilangowski and coworkers [18] that Na diffusion becomes increasingly retarded by correlation effects with increasing X_K. This proposition is corroborated by the fact that $D^*_{Na}(MO) < D^*_{Na}(VF)$ where $X_K(MO) = 0.95$ and $X_K(VF) = 0.83$, but it is in conflict with our finding that $D^*_{Na}(VF) \approx 100 D^*_{Na}(AZ)$ despite nearly identical compositions, i.e. the X_K values, of these feldspars. Finally, the fact that $D^*_{Na}(RK) \approx D^*_{Na}(VF)$, despite a significant difference in their compositions, $X_K(RK) = 0.71$ and $X_K(VF) = 0.83$, is striking and requires an alternative explanation. It is thus inferred that over the compositional range $0.71 \leq X_K \leq 0.94$, which is covered by our experiments combined with the literature data, the major element composition expressed by X_K is not the dominant parameter, which controls Na diffusion in the K-rich alkali feldspars.

Moreover, in the group VF & RK, an increase of X_K from 0.71 to 0.83 enhances the rate of Na diffusion, whereas an increase of X_K from 0.835 to 0.95 reduces the rate of Na diffusion in the group AZ & MO. Thus, different factors influence Na diffusion in these two groups of feldspars.

Alkaline impurities. A certain impact might be expected from the alkaline earth elements Ba and Ca, which are present as divalent cations at low concentrations and may enter the crystal structure of the alkali feldspars via heterovalent substitution, replacing monovalent Na or K on the alkali sublattice. Such substitution may be charge-balanced by coupled substitution of three-valent Al for

tetra-valent Si on the tetrahedral sites. Alternatively, such a substitution may be compensated by the formation of vacancies on the alkali sites, which would enhance the diffusion of alkali cations via vacancies. The Ba and Ca contents of AZ and VF are, however, rather similar (see Table I), and vacancies created due to the heterovalent substitution cannot explain the strongly different Na diffusivities in these two feldspars (Fig. 8).

Al/Si ordering. According to the Kroll and Ribbe classification, the b/c relation for Adularia is equal to 0.88 while for Madagascar it is equal to 0.69 [27]. In view of the classification of Jones [28], we may expect a higher degree of Al/Si ordering in the AZ and MO feldspars than in the VF and RK feldspars. Thus, we infer that an increase of the Al/Si disorder in alkali feldspars leads to an increase in the Na diffusion rates. Noting that the difference in Na diffusivites between AZ and VF, with nearly identical X_{K} but with substantially different degrees of the Al/Si ordering, is three orders of magnitude, we infer that the degree of the Al/Si ordering dominates strongly Na diffusion in alkali feldspar. The degree of Al/Si ordering is comparable for AZ and MO. The fact that the Na diffusivity in the relatively Na-rich AZ, $X_{\mathrm{K}}(\mathrm{AZ}) = 0.85$, is higher than in the comparatively Na-poor MO, $X_{\mathrm{K}}(\mathrm{MO}) = 0.95$, indicates that for feldspars with comparable degree of Al/Si ordering, an increase in X_{K} leads to a decrease of the Na diffusion coefficients.

One may propose a qualitative description of the influence of Al/Si order on the Na diffusion rates following the phenomenological approach proposed by Girifalco for diffusion in ordered metallic alloys [29]. Assuming a vacancy diffusion mechanism, the impact of solely Al/Si ordering on the activation energy, Q, of Na diffusion in a feldspat is then simply

$$Q = Q_0 \left(1 + \alpha_1 S_1^2 + \alpha_2 S_1^2\right) \tag{4}$$

where Q_0 is the activation energy of Na diffusion in a fully disordered state, $S_1 = S_2 = 0$, and S_1 and S_2 are the order parameters defined as $S_1 = X_{\mathrm{Al}}^{\mathrm{T_1}} - X_{\mathrm{Al}}^{\mathrm{T_2}}$ and $S_2 = X_{\mathrm{Al}}^{\mathrm{T_{1o}}} - X_{\mathrm{Al}}^{\mathrm{T_{1m}}}$. α_1, α_2 are numerical constants. Here $X_{\mathrm{Al}}^{\mathrm{T_1}}$ ($X_{\mathrm{Al}}^{\mathrm{T_2}}$) is the fraction of Al atoms on the T_1 (T_2) sites and $X_{\mathrm{Al}}^{\mathrm{T_{1o}}}$ ($X_{\mathrm{Al}}^{\mathrm{T_{1m}}}$) is their subfraction with preferential substitution of the $T_{1\mathrm{o}}$ ($T_{1\mathrm{m}}$) sites. According to this definition, the partially and fully ordered states correspond to $S_1 = 1$ & $S_2 = 0$ and $S_1 = S_2 = 1$ combinations, respectively. Note that according to the above definitions, $X_{\mathrm{Al}}^{\mathrm{T_1}} + X_{\mathrm{Al}}^{\mathrm{T_2}} = 1$ and $X_{\mathrm{Al}}^{\mathrm{T_{1o}}} + X_{\mathrm{Al}}^{\mathrm{T_{1m}}} = 1$.

Phenomenologically, the parameters α_1 and α_2 account for the increase of the alkali vacancy migration (and potentially also the formation) energies due to the Al/Si ordering. The potential impact of the Al/Si ordering on the Na diffusion rates can be quantified via dedicated ab initio calculations, especially with respect to the defect formation and migration energies.

IV. CONCLUSIONS

The Na diffusion coefficients were determined for single crystalline alkali feldspars using the ^{22}Na radiotracer experiments. The investigated feldspars cover a compositional range of $0.71 \leq X_{\mathrm{K}} \leq 0.95$ and exhibit different degrees of Al/Si ordering and minor element contents (alkaline impurities). The experiments were performed at temperatures ranging from about 800 K to 1200 K and the Na diffusivites were determined for specific crystallographic directions. All measurements considered in this study follow the same experimental protocol, which ensures a high internal reproducibility. The main results can be summarized as follows:

- Comparison of the Na diffusivites in alkali feldspars obtained from the same experimental approach reveals relatively fast Na diffusion in the VF and RK feldspars and comparatively slow Na diffusion rates in the MO and AZ feldspars. We suggest that the systematic difference of the Na diffusion rates is due to the differences in the state of Al/Si ordering, which appears to exert a first-order control on Na diffusion in alkali feldspar.

- The K-site fraction on the alkali sites influences Na diffusion in alkali feldspar, too, but this effect is subordinate to the degree of Al-Si ordering over the investigated compositional range. It is thus prominent only when Na diffusion rates in alkali feldspars with comparable degrees of Al/Si ordering are examined. The degrees of Al/Si ordering are similar for the MO & AZ feldspars, and comparison of the Na diffusivities measured in these two feldspars indicates that Na diffusion becomes more sluggish with increasing K-site fraction. This is proposed to be explained by the correlation effects which become more pronounced with increasing site fraction of the relatively immobile K cation and in the case of the MO & AZ feldspars this factor is particularly effective at a K-site fraction of 0.95.

- The Na diffusion rates along the normal directions to the (001) and (010) crystallographic planes in Madagaskar orthoclase (MO) and Adularia from Zillertal (AZ) are rather similar. In the MO feldspar, the Na diffusivites in these two directions are indistinguishable, in the AZ feldspar, the Na diffusivity normal to the (001) crystallographic plane is faster than that normal to the (010) plane by a factor of two to three. For the MO feldspar, the Na diffusivites were determined in six different crystallographic directions, and the full tensor of Na tracer diffusion in the K-rich alkali feldspar was determined. Nearly isotropic diffusion in the (100) plane, which contains the normal directions to the (001) and (010) planes, is revealed, but Na diffusion in the directions strongly inclined to the

(100) plane is comparatively fast at low temperatures and comparatively slow at high temperatures. This implies a diffusion anisotropy in the (010) plane, which changes with temperature. We propose that this behavior reflects different activation energies, and supposedly different underlying mechanisms, for Na diffusion in the (100) plane and in the directions pointing out of the (100) plane.

Acknowledgments. The paper is written in memory of a great scientist and distinguished personality, Prof. Dr. Nicolaas Stolwijk (Nico), who contributed a lot to the current understanding of tracer diffusion in the feldspars. Financial support from the German Science Foundation (DFG) via research grant DI 1419/18-1 and Austrian Science Fund (FWF) via research grant I4404 is acknowledged. We thank Gerald Giester for help with single crystal X-ray diffraction experiments and Jürgen Schreuer for providing VR, RK and MO feldspar.

[1] R.A. Yund. *Alkali Feldspar Exsolution: Kinetics and Dependence on Alkali Interdiffusion*, pages 281–315. Springer Netherlands, Dordrecht, 1984.

[2] E. Petrishcheva, L. Tiede, K. Schweinar, G. Habler, C. Li, B. Gault, and R. Abart. Spinodal decomposition in alkali feldspar studied by atom probe tomography. *Physics and Chemistry of Minerals*, 47:30, 2020.

[3] D. González-Garcia, M. Petrelli, H. Behrens, F. Vetere, L.A. Fischer, D. Morgavi, and D. Perugini. Diffusive exchange of trace elements between alkaline melts: Implications for element fractionation and timescale estimations during magma mixing. *Geochimica et Cosmochimica Acta*, 233:95–114, 2018.

[4] F. Costa, T. Shea, and T. Ubide. Diffusion chronometry and the timescales of magmatic processes. *Nat Rev Earth Environ*, 1:201–214, 2020.

[5] F. Costa. Clocks in magmatic rocks. *Annual Review of Earth and Planetary Sciences*, 49(Volume 49, 2021):231–252, 2021.

[6] C. Ferrando, K.J. Lynn, V. Basch, B. Ildefonse, and M. Godard. Retrieving timescales of oceanic crustal evolution at oceanic core complexes: Insights from diffusion modelling of geochemical profiles in olivine. *Lithos*, 376-377:105727, 2020.

[7] S. Chakraborty and R. Dohmen. Diffusion chronometry of volcanic rocks: looking backward and forward. *Bull Volcanol*, 84:57, 2022.

[8] J.B. Brady and D.J. Cherniak. Diffusion in Minerals: An Overview of Published Experimental Diffusion Data. *Reviews in Mineralogy and Geochemistry*, 72(1):899–920, 01 2010.

[9] F. Laves. The feldspars, their polysynthetic twinning and their phase relations. *Rendiconti della Societa Italiana di Mineralogia e Petrologia*, 16:37–100, 1960.

[10] A.R. Philpotts and J.J. Ague. *Principles of Igneous and Metamorphic Petrology*. Cambridge University Press, 3rd edition, 2022.

[11] J.G. Moore and T.W. Sisson. Igneous phenocrystic origin of K-feldspar megacrysts in granitic rocks from the Sierra Nevada batholith. *Geosphere*, 4:387–400, 2008.

[12] B.J. Giletti and T.M. Shanahan. Alkali diffusion in plagioclase feldspar. *Chemical Geology*, 139(1):3–20, 1997.

[13] E. Petrishcheva, L. Tiede, D. Heuser and· H. Hutter, G. Giester, and R. Abart. Multicomponent diffusion in ionic crystals: theoretical model and application to combined tracer- and interdiffusion in alkali feldspar. *Physics and Chemistry of Minerals*, 47:35, 2020.

[14] F. Wilangowski. *The Interstitialcy Diffusion Mechanism in Alkali Feldspar: Self-Diffusion Measurements and Monte Carlo Simulations*. PhD thesis, PhD thesis, University of Münster, Germany, 2017.

[15] B. Tas Kavakbasi. *Temperature and Orientation dependence of ^{22}Na tracer diffusion in Madagascar K-feldspar*. PhD thesis, Master thesis, University of Münster, Germany, 2015.

[16] A. Knieschewski. *Sodium radiotracer diffusion in single crystal alkali feldspar*. PhD thesis, Master thesis, University of Münster, Germany, 2015.

[17] F. Hergemöller, M. Wegner, M. Deicher, H. Wolf, F. Brenner, H. Hutter, R. Abart, and N.A. Stolwijk. Potassium self-diffusion in a K-rich single-crystal alkali feldspar. *Phys Chem Minerals*, 44:345–351, 2017.

[18] F. Wilangowski, R. Abart, S.V. Divinski, and N.A. Stolwijk. Radiotracer experiments and monte carlo simulations of sodium diffusion in alkali feldspar: Evidence against the vacancy mechanism. In *Diffusion in Materials*, volume 363 of *Defect and Diffusion Forum*, pages 79–84. Trans Tech Publications Ltd, 6 2015.

[19] W.L. Brown and I. Parsons. Alkali feldspars: ordering rates, phase transformations and behaviour diagrams for igneous rocks. *Mineralogical Magazine*, 53(369):25–42, 1989.

[20] D. Heuser, E. Petrishcheva, F. Ingegneri, C. L. Lengauer, E. Dachs, C. Hauzenberger, and R. Abart. Thermodynamic mixing properties of disordered alkali feldspar solid-solution from na–k partitioning and low-temperature calorimetry. *Physics and Chemistry of Minerals*, 51(1):9, 2024.

[21] Y. Yang, Y. Min, J. Lococo, and Y.-S. Jun. Effects of al/si ordering on feldspar dissolution: Part i. crystallographic control on the stoichiometry of dissolution reaction. *Geochimica et Cosmochimica Acta*, 126:574–594, 2014.

[22] S. Liu and Y Zhai. Degree of Al-Si order in K-feldspar and its effect on K-feldspar's dissolution. *Period. Mineral.*, 90:359–369, 2021.

[23] D. Gaertner, L. Belkacemi, V.A. Esin, F. Jomard, A.A. Fedotov, J. Schell, J.V. Osinskaya, A.V. Pokoev, C. Duhamel, A. Paul, and S.V. Divinski. Techniques of tracer diffusion measurements in metals, alloys and compounds. *Diffusion Foundations*, 29:31–73, 5 2021.

[24] E. Petrishcheva, R. Abart, A.-K. Schäffer, G. Habler, and D. Rhede. Sodium-potassium interdiffusion in potassium-rich alkali feldspar I: Full diffusivity tensor at 850°C. *American Journal of Science*, 314(9):1284–1299, 2014.

[25] H. Kroll, I. Schmiemann, and G. von Cölln. Feldspar solid solutions. *Am. Mineral.*, 71:1–16, 1986.

[26] H. Behrens, W. Johannes, and H. Schmalzried. On

the mechanisms of cation diffusion processes in ternary feldspars. *Physics and Chemistry of Minerals*, 17(1):62–78, 1990.

[27] H. Kroll and P. Ribbe. *Lattice Parameters, Composition and Al/Si Order in Alkali Feldspars*. in Feldspar Mineralogy, (ed) P. Ribbe, Mineralogical Society of America, 1983.

[28] J. Jones. Order in Alkali Feldspars. *Nature*, 210:1352–1353, 1966.

[29] L.A. Girifalco. Vacancy concentration and diffusion in order-disorder alloys. *Journal of Physics and Chemistry of Solids*, 25(3):323–333, 1964.